Laser and Particle Beams (2012), *30*, 559–567.

doi:10.1017/S0263034612000560

Molybdenum thin films via pulsed laser deposition technique for first mirror application

A.T.T. MOSTAKO AND ALIKA KHARE

Laser and Photonics laboratory, Department of Physics, Indian Institute of Technology Guwahati, Guwahati, India

(RECEIVED 7 April 2012; ACCEPTED 12 July 2012)

Abstract

Mirror like Molybdenum thin films on SS substrate in vacuum (10^{-3} Pa) and in Helium environment has been achieved by Pulsed Laser Deposition (PLD) Technique. The PLD thin films of Molybdenum have been characterized by using X-ray Diffraction (XRD) pattern, Scanning Electron Microscope (SEM), Atomic Force Microscope (AFM) and Energy Dispersive X-ray (EDX). The specular reflectivity was recorded with Fourier Transform Infra-Red spectrometer and UV-Visible spectrometer. The optical quality of the thin films was tested via interferometric technique. At the optimum deposition parameters, the crystal orientation was in Mo(110) phase. The FIR-UV-Visible reflectivity of the mirror was found to be closed to that of the polished bulk Molybdenum and Stainless Substrate (SS) substrate.

Keywords: First mirror; Molybdenum; Pulsed laser deposition; Reflectivity; Thin films

1. INTRODUCTION

The optical diagnostics of confined fusion plasma plays an important role to understand the performance of Fusion devices (e.g., International Thermonuclear Experimental Reactor) (Marot *et al.*, 2008). The plasma facing mirrors in the optical diagnostic system of these fusion devices are known as first mirrors (FMs). FMs are one of the most critical elements of optical diagnostics systems of fusion device. FMs have to withstand the harsh environment arising from electromagnetic radiation and bombardment of particles (neutrons, charge exchange atoms) from high temperature plasma (Zhou *et al.*, 2006). The long term exposure of the mirrors under such harsh environment deteriorates its surface quality. The main causes for the degradation of FMs under long term diagnostic operation are: (1) erosion and redeposition processes due to bombardment of charge exchange atoms, (2) volumetric swelling due to neutron flux, and (3) mirror surface heating due to X-ray and ultraviolet (UV) radiation (Voitsenya *et al.*, 1999, 2001). It is reported that even a 10–20 nm thick contaminated impurities onto the mirrors can drastically change the optical property of metal mirrors (Voitsenya *et al.*, 2001). It has been shown that mirrors of mono-crystalline refractory metals (Mo, W, Rh) can have sufficiently long life time as a FM in fusion devices (Voitsenya *et al.*, 2001). The growth of the bulk crystal of heavy elements such as Mo, W, Rh, etc., with good polished surface is a difficult task. Therefore, fabrication and testing of mirrors made from thin films of these metals as an alternative have generated intensive research interest (Voitsenya *et al.*, 1999, 2001; Marot *et al.*, 2008). The reflectivity of these films is comparable to that of polished bulk crystal (Voitsenya *et al.*, 2001). These thin metal films also possess high electrical conductivity, excellent mechanical strength, high melting point, good metal barrier performance, and fine pattern ability (Shen *et al.*, 2000; Djerdj *et al.*, 2005). Due to high reflectivity in the far infra red (FIR) and UV-visible range, Molybdenum (Mo) mirror is an attractive candidate for FMs in fusion devices (Lipa *et al.*, 2006; Voitsenya *et al.*, 2001). Besides this, Mo is widely used as an alloying addition in stainless steels (SS) to facilitate the formation of the passive film and to improve resistance to pitting attack (Tomachuk *et al.*, 2003). Also, Mo thin films are used for NO gas detection, the back contact in thin film solar cells, micro-electronics and semiconductor industries (Tomachuk *et al.*, 2003). Mo thin films prepared by direct current and radiofrequency magnetron sputtering technique (Hirata *et al.*, 1990; Khatri *et al.*, 2008) and chemical vapor deposition (Gesheva *et al.*, 1992; Juppo *et al.*, 1998) are well documented in literature. There are few reports on the Mo thin films fabricated via pulsed laser deposition (PLD) technique (Fruchart *et al.*, 1998). PLD is highly flexible technique that can be applied to any material (Shukla *et al.*,

Address correspondence and reprint requests to: Alika Khare, Department of physics, Indian Institute of Technology Guwahati, Guwahati-781039, India. E-mail: alika@iitg.ernet.in

2010; Wolowski *et al.*, 2007; Lam *et al.*, 2007). Besides this, pulsed laser ablation has potential application toward intense heavy ion generation and acceleration (Orlov *et al.*, 2011; Roth *et al.*, 2005), nanoparticle synthesis (Nath *et al.*, 2011; Wang *et al.*, 2011), and laser ablation lithography (Kamlesh *et al.*, 2006).

In this work, PLD technique was used to deposit mirror like Mo thin film on SS substrate. The effect of target-substrate distance and background Helium gas pressure on surface morphology, FIR and UV-visible reflectivity of the mirror like PLD thin films of Mo is reported.

2. EXPERIMENTAL SETUP

The experimental set up used for PLD of Mo thin films is shown in Figure 1. The high power laser beam (second harmonic of *Q*-switched Nd:YAG laser, Model: Quanta systems-HYL101, 450 mJ/pulse in fundamental with about 10 ns pulse duration and 10 Hz repetition rate) was steered with a high damaged threshold right angled prism into the deposition chamber and loosely focused by a lens of 35 cm focal length onto Mo target. The Mo target in the form of a strip of size 50 mm × 10 mm and thickness 1 mm, purity 99.95%, was mounted inside the ablation chamber with a motorized translated stage. Focusing of high power laser leads to luminous high temperature plasma formation of Mo. This plasma expands hemi-spherically (Kamlesh *et al.*, 2005) and perpendicularly to the surface of the target in vacuum, cools down and gets deposited onto the SS substrate placed parallel to and few cm apart from the target. The continuous translation of the target during the deposition process provides the fresh target surface on shot to shot basis of the laser beam. The SS substrates of size 10 mm × 10 mm were polished by abrasive high precession polishing machine and were cleaned by usual substrate cleaning protocols before deposition. Prior to PLD, the ablation chamber and substrate heater during evacuation was baked (about 12 h) for removal of residual oxygen and water vapor to prevent the oxides formation of Mo. The Mo films were deposited at elevated substrate temperature of 773° K to improve the film-substrate adhesion and to reduce root mean square (RMS) roughness. The effect of target-substrate distance onto the PLD thin films of Mo studied under vacuum (about 10^{-3} Pascal). From this, the optimized target-substrate distance was obtained best quality thin film. The effect of Helium gas pressure onto the quality of PLD Mo thin films at this optimized distance was studied. For this, Mo thin films were fabricated at five different Helium gas pressures; 5, 10, 50, 100, and 200 Pascal.

All the Mo thin films were deposited under loosely focused condition of the laser beam so as to minimize the formation of liquid droplets. The prime reasons for the formation of liquid droplet and microstructure with very high fluence of laser are due to the tight focusing of the laser beam onto the target. Tight focusing of the laser beam leads to three type of instabilities during ablation and plasma formation process: (1) Instabilities of the plane front of liquid evaporation due to spatial modulation of the pressure in the near surface plasma layer, followed by melt outflow from pits to humps and subsequent solidification, (2) Rayleigh-Taylor type instability at liquid-vapor interface due to multi-pulse relief formation, and (3) Kelvin-Helmholtz type instability when vapor velocity is much higher than the liquid layer velocity (Brailovsky *et al.*, 1995). The loosely focused laser beam results into the lower fluence and hence the evaporation of the target material extended to larger laser spot area which results to a low energetic plasma plume (Kamlesh *et al.*, 2005, 2006). The single shot laser beam spot size is shown in Figure 2. The major and minor diameters of laser spot are 1808.6 μm and 1315.3 μm, respectively. This corresponds to the laser fluence of 21 kJ/m^2.

Thickness of Mo thin films was measured by stylus profilometer with a 12.5 μm diamond tip. For this, the films were

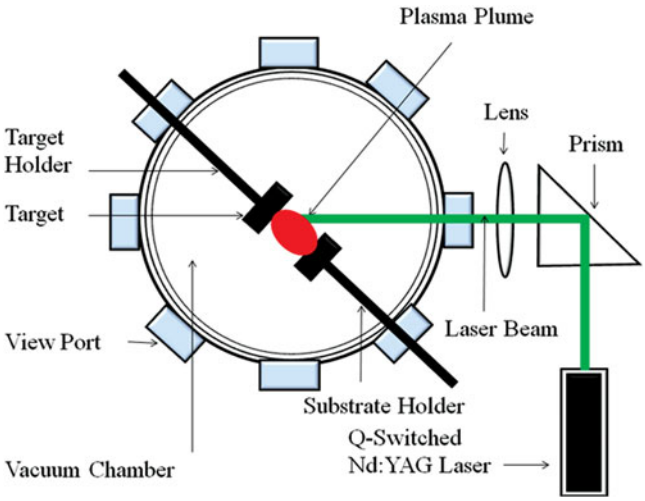

Fig. 1. (Color online) Schematic diagram of experimental PLD set up.

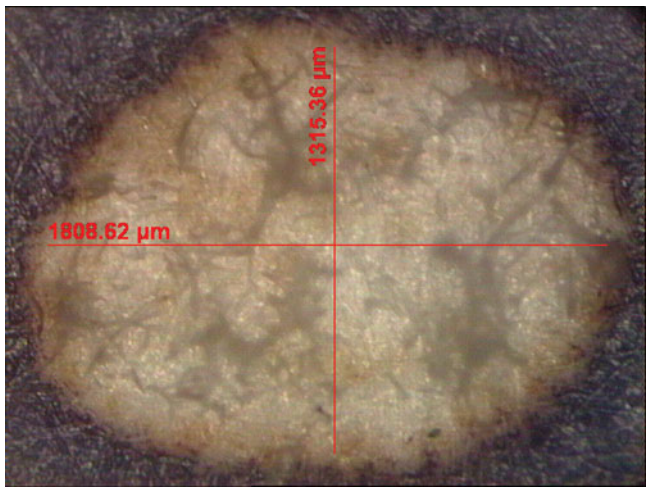

Fig. 2. (Color online) Micrograph of laser beam Spot size.

https://doi.org/10.1017/S0263034612000560 Published online by Cambridge University Press

partially deposited by placing a copper mask onto the SS substrate. Thus, a substrate-film step was formed on it. In the profilometer set-up, the substrate-film step was scanned linearly at three different places. Surface morphology of the Mo thin films was studied with scanning electron microscope (SEM). Film composition was identified using energy dispersive X-ray (EDX). The crystal structure of mirror like Mo thin film was analyzed using X-ray diffraction (XRD) pattern. The specular reflectivity of the Mo thin films were recorded at 17.5° incidence angle with Fourier transforms infra red (FTIR) spectrometer. The UV-visible reflectivity was recorded at 45° incidence angle. The fringe visibilities of the SS substrates and Mo thin films were tested by interferometric technique (Hernandez *et al.*, 1999). For this, one of the mirrors of the Michelson interferometer was replaced with PLD thin film of Mo. Interference pattern was recorded onto a CCD (PixelFly, PCO, 230 XS 1839) for the measurement of fringe visibility.

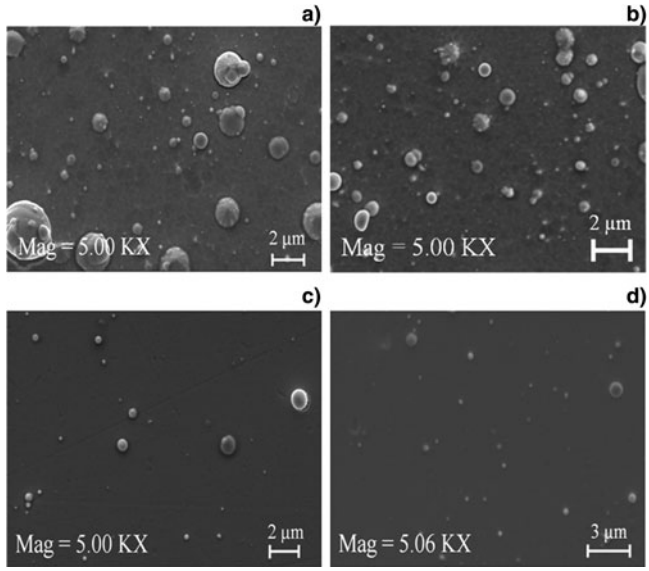

Fig. 3. SEM image of the samples (**a**) Mo_1, (**b**) Mo_2, (**c**) Mo_3, and (**d**) Mo_4, respectively.

3. RESULTS AND DISCUSSION

The sample codes assigned to PLD of Mo thin films, at various target-substrate distances are listed in Table 1.

3.1. Effect of Target-Substrate Distance onto the Quality of the Mo Thin Films

3.1.1. Surface Morphology

The SEM images at about 5 kX magnifications of mirror like PLD thin films of Mo deposited for 3 h on polished SS substrate for samples Mo_1, Mo_2, Mo_3, and Mo_4 are shown in Figure 3. The corresponding EDX spectra are shown in Figure 4. The average size of grain formed due to the deposition of liquid droplets obtained from the SEM image analysis is listed in Table 1. Mo_1 film shows formation of large grains and microstructure (Fig. 3a). The average grain size was about 1.8 μm. This particular film was deposited at target-substrate distance (D_{TS}) 0.02 m. The smallest grain size due to the deposition of liquid droplet was observed for Mo_4 thin film, which was deposited at D_{TS}: 0.05 m. The average size of the liquid droplet for this film was 0.5 μm. With the increase of target-substrate distances, Figure 3 the grain size and microstructure decreases due to the fragmentation into smaller droplet before deposition onto the surface at large target-substrate distances. The EDXs of Mo_1, Mo_2, Mo_3, and Mo_4 confirm the presence of Mo and absence of substrate constituent elements (Fe, Cr) and impurities: carbon, oxygen. The EDX of Mo thin film deposited at $D_{TS} = 0.06$ m showed the substrate constituent elements and beyond this distance, Mo could not be detected, as the longitudinal plasma density falls down nearly exponentially with the increase of target-substrate distance. Thus the deposition of the Mo thin film at $D_{TS} = 0.06$ m is very low and beyond the detection limit of the probing electron of EDX. Therefore, the upper limit of the target-substrate distance was limited to 0.05 m in the present studies.

The AFM images of Mo_1, Mo_2, Mo_3, and Mo_4 are shown in Figure 5. The RMS roughness of the corresponding films averaged over three different scan areas of size 2 μm × 2 μm

Table 1. *Sample code, target-substrate distance (D_{TS}), FWHM of (110) peak of Mo, Radius of curvature (r), average grain size, RMS roughness at 2 μm × 2 μm (q), Reflectivity (% R), and Fringe Visibility (V)*

Sample Code	D_{TS} (m)	FWHM	r (m)		Grain size (μm)	q (nm)	% R		V
			before	after			at λ = 20 μm	at λ = 840 nm	
Mo_1	0.02	No peak	4.6	4.7	1.8	49	91	55	0.61
Mo_2	0.03	1.4°	3.5	3.0	1.3	21	93	69	0.72
Mo_3	0.04	0.8°	5.2	5.1	0.7	17	94	67	0.73
Mo_4	0.05	0.7°	5.4	5.6	0.5	9	95	70	0.80
Mo Bulk		0.2°	—			—	95	73	—
SS substrate		—	—			—	93	79	0.77
Standard mirror		—	Very large (Straight fringe)			—	—	—	0.84

https://doi.org/10.1017/S0263034612000560 Published online by Cambridge University Press

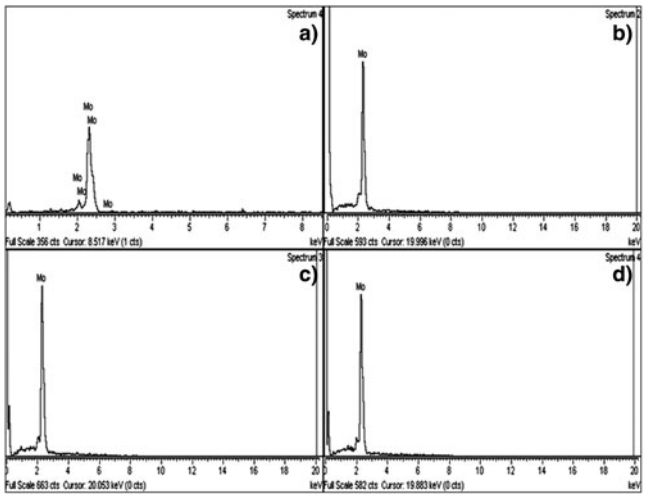

Fig. 4. EDX of the samples (**a**) Mo_1, (**b**) Mo_2, (**c**) Mo_3, and (**d**) Mo_4, respectively.

are listed in Table 1. The Mo_1 sample shows maximum (49 nm) RMS roughness while that of Mo_4 shows minimum (9 nm) RMS roughness. The RMS roughness data presented in Table 1 clearly shows that the surface morphology of the films improves with the increase of target-substrate distance. Due to the expansion, the arriving Mo plasma plume substrate is more uniformly distributed at larger target-substrate distance and hence the RMS roughness reduces.

3.1.2. Structural Characterization

The XRD pattern of Mo_1, Mo_2, Mo_3, Mo_4, and polished bulk Mo mirror is shown in Figure 6. The Mo_1 shows no prominent crystal orientation except that of the substrate. The Mo_2, Mo_3, and Mo_4 thin films show prominent crystal orientation of (110) plane of Mo along with small peak of (200)

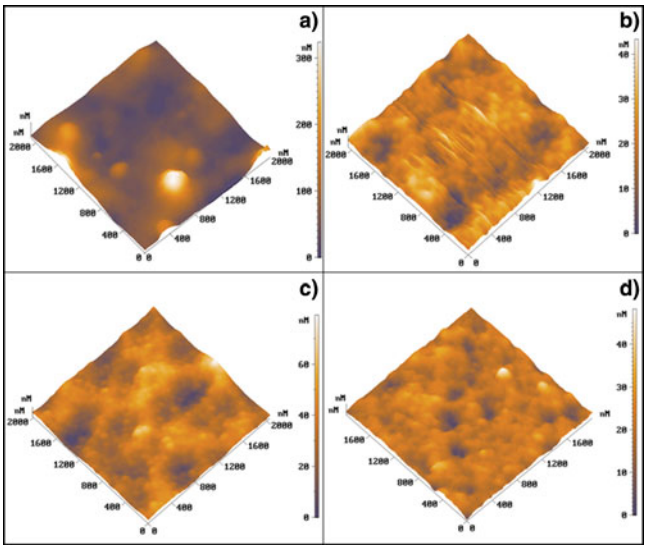

Fig. 5. (Color online) AFM image of the samples (**a**) Mo_1, (**b**) Mo_2, (**c**) Mo_3, and (**d**) Mo_4, respectively.

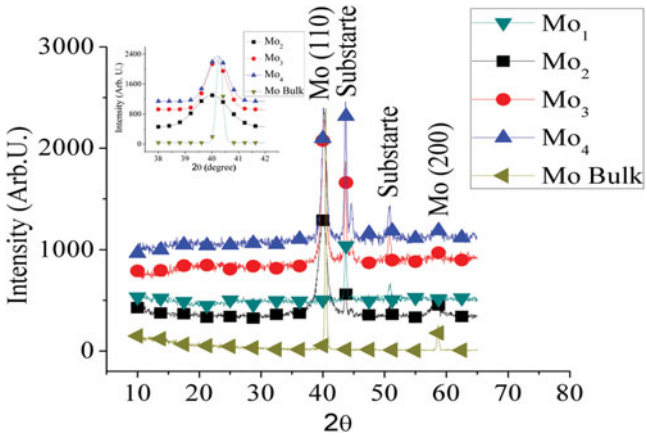

Fig. 6. (Color online) XRD patterns of the samples Mo_1, Mo_2, Mo_3, Mo_4, and bulk Mo mirror.

orientation. The inset in Figure 6 shows the enlarge view of the XRD pattern for (110) plane of Mo from $2\theta = 38°$ to 42°. The full width at half maximum (FWHM) of these samples are listed in Table 1. The FWHM decreases with the increase of target-substrate distance. It was 1.4° for Mo_2 and 0.7° for that of Mo_4, respectively. The FWHM of polished Mo target was 0.2°. The broadening of XRD peak in the PLD thin films is due to the cumulative effect of stress present in the film, formation of nanomicro structures and the amorphous nature of the film (Culity, 1956). The decrease in FWHM with increase of target-substrate distance is due to cumulative effect of the lowering of stress present in the film and decrease of size of the liquid droplets with the increase of target-substrate distance. The kinetic energy of the ablated species in the plasma plume decreases with the increase of target-substrate distance. Therefore, the ablated species striking the substrate with low kinetic energy at large target-substrate distance and hence reduces the stress in the film. Moreover, the ejected liquid droplet from the target gets enough time for fragmentation that results in the decrease of the size of the liquid droplet. The XRD pattern as shown in Figure 6 further confirms the absence of Molybdenum oxide formation.

3.1.3. FIR and UV-visible Reflectivity

The specular FIR reflectivity in the spectral range of 1.4 μm to 25 μm for all the samples and polished bulk Mo mirror are shown in Figure 7a. The UV-visible reflectivity from $\lambda = 350$ nm to $\lambda = 1150$ nm of these samples are shown in Figure 7b. The reflectivity at $\lambda = 20$ μm and at $\lambda = 840$ nm is listed in Table 1. It confirms that the reflectivity increases with target-substrate distance. The good surface morphology (Figs. 3 and 5) is the prime factor for the increase in mirror reflectivity. The reflectivity of Mo_2 and Mo_3 film approaches to that of SS substrate and the mirror made of polished bulk Mo. The Mo_4 thin film and polished bulk Mo mirror shows maximum reflectivity (about 95% at $\lambda = 20$ μm). This particular film was deposited at $D_{TS} = 0.05$ m and has lowest

https://doi.org/10.1017/S0263034612000560 Published online by Cambridge University Press

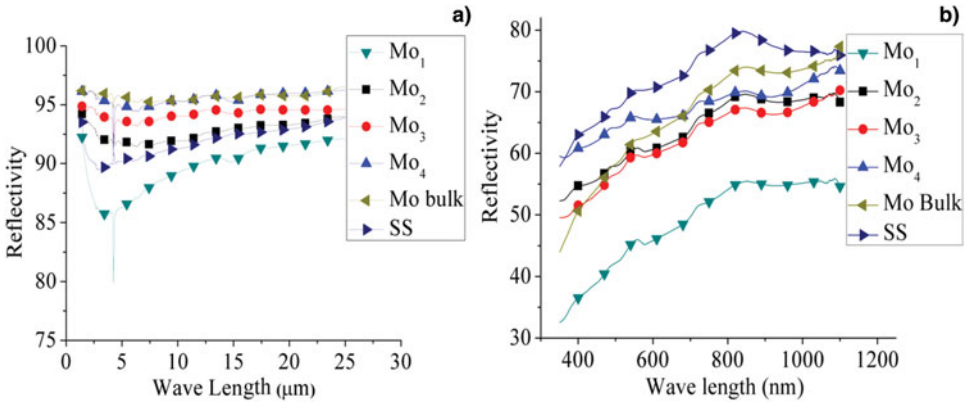

Fig. 7. (Color online) (**a**) The specular FTIR reflectivity of the samples Mo_1, Mo_2, Mo_3, Mo_4, SS-substrate and Bulk Mo mirror (**b**) The corresponding UV-visible reflectivity.

RMS roughness. The Mo_1 thin film deposited at D_{TS} = 0.02 m shows minimum reflectivity in FIR and UV-visible range as its surface is very rough due to the deposition of micron sized liquid droplets. The sharp dip in specular reflectivity at $\lambda = 4.258$ μm is due the substrate only as SS has strong absorption around this wave length.

3.1.4. Fringe Visibility

The interference patterns of PLD Mo mirror (after deposition) and corresponding SS substrate (before deposition) are shown in Figure 8 for samples Mo_1–Mo_4, respectively. The radius of curvature and the fringe visibility of the PLD mirrors of Mo obtained from respective interference patterns are listed in Table 1. The curved fringes are due to the curvature present in the corresponding substrate, initially, before deposition. The marginal changes in radius of curvature of the Mo thin films to its corresponding substrate confirmed the uniform deposition within substrate area. The distinct interference pattern of the thin films confirms that PLD Mo thin film possess mirror like quality. The fringe visibility of the interference pattern obtained from the mirror like Mo thin films, standard mirror and polished SS substrate is listed in Table 1. The fringe visibility of the Mo_4 thin film is 0.80 and close to that obtained by the standard mirror 0.84. The data presented in Table 1 shows fringe visibility of the thin film increases with the target-substrate distance. It is again due to the improvement of mirror like quality (smooth surface morphology) with the increase of target-substrate distance.

3.2. Effect of Background Helium onto the Quality of Mo Thin Films

The presence of inert gas during the laser ablation helps in plasma confinement and cooling. Therefore, the kinetic energy of the ablated atoms propagating toward the substrate reduces. This prohibits the sputtering of the film deposited on shot to shot basis and hence the surface roughness reduces. As the films deposited under vacuum at D_{TS}: 0.03 and 0.04 m were of better quality, therefore to study the effect of background helium gas pressure onto the quality of the thin films, a systematic variation of gas pressure 5, 10, 50, 100, and 200 Pascal at D_{TS}: 0.03 and 0.04 m only was performed. The detail deposition parameters of these samples

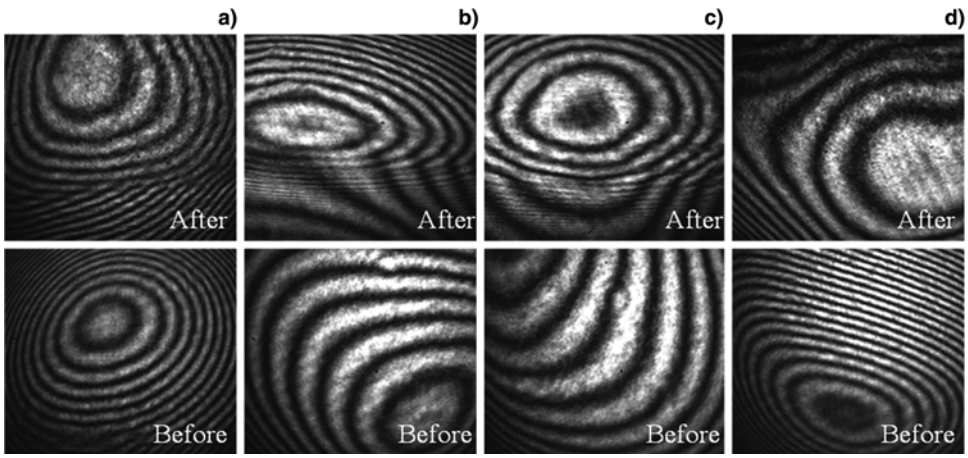

Fig. 8. Interference pattern of the samples (**a**) Mo_1, (**b**) Mo_2, (**c**) Mo_3, and (**d**) Mo_4 before and after deposition, respectively.

https://doi.org/10.1017/S0263034612000560 Published online by Cambridge University Press

Table 2. *Sample code, target-substrate distance (D_{TS}), Helium ambient (B_p), thickness (t), FWHM of XRD peak (110) of Mo, Reflectivity (% R)*

Sample Code	D_{TS} (m)	B_p (Pascal)	t (nm)	FWHM	% R	
					at λ = 20 μm	at λ = 840 nm
Mo_5	0.03	5	296	0.6°	96	42
Mo_6	0.03	10	308	0.6°	98	49
Mo_7	0.03	50	386	0.6°	98	83
Mo_8	0.03	100	252	0.7°	97	84
Mo_9	0.03	200	242	No peak	95	71
Mo_{10}	0.04	5	229	0.7°	93	59
Mo_{11}	0.04	10	231	0.7°	95	63
Mo_{12}	0.04	50	322	0.5°	98	87
Mo_{13}	0.04	100	265	1.2°	98	79
Mo_{14}	0.04	200	240	No peak	88	67

are listed in Table 2. The deposition time for all these films was maintained at one hour.

3.2.1. *Thickness*

The measured thickness (averaged over three different locations) of the Mo_5–Mo_9 deposited at D_{TS}: 0.03 m and Mo_{10}–Mo_{14} at D_{TS}: 0.04 m thin films are listed in Table 2. The variation of thickness with deposition background gas pressure for the films Mo_5–Mo_9 and Mo_{10}–Mo_{14} are shown in Figure 9. It was observed that the thickness of the Mo thin films increases initially with Helium pressure to 50 Pascal gas pressure and then slowly decreased with the further increase of gas pressure up to 200 Pascal. This behavior is due to the confinement of the laser induced plasma with the increase of background pressure. Initially, when the background pressure is low, the confinement taking place within a hemispherical region was comparable to that of the target-substrate distance. Therefore, the plasma density increased with the confinement of the plasma which increased the deposition rate on the substrate and hence increase in thickness. With the further increase of background pressure, the plasma was confined to smaller region, than the target-substrate distance. Thus, there is a significant decrease in the laser ablated species reaching towards substrate which decreased the deposition rate and hence thickness of the film. The maximum thickness, 386 nm was observed for Mo_7 thin films deposited at D_{TS}: 0.03 m. The deposition rate of this thin film, deposited around 50 Pascal, is about 6 nm/min where as that of the films deposited under vacuum is about 4 nm/min at 0.03 m target-substrate distance. The thickness of the films at D_{TS}: 0.03 m was more under same background pressure than that of the films deposited at D_{TS}: 0.04 m.

3.2.2. *Structural Characterization*

The XRD pattern of Mo_5–Mo_9 and Mo_{10}–Mo_{14} are shown in Figure 10. The prominent Mo (110) crystal orientation along with small peak of Mo (200) orientation and two substrate peaks for Mo_5–Mo_8 and Mo_{10}–Mo_{13} were confirmed from their respective XRD patterns. The FWHM of Mo (110) XRD peak for Mo_5–Mo_8 and Mo_{10}–Mo_{13} are listed in Table 2. The FWHM data presented in Tables 1 and Table 2 confirms the overall improvement in the Mo (110) crystal orientation with Helium pressure in the range of 5 and 50 Pascal. The FWHM of Mo (110) XRD peak for Mo_{13} is 1.2°. The poor crystalline nature of this thin film could be due to the low kinetic energy of the laser ablated

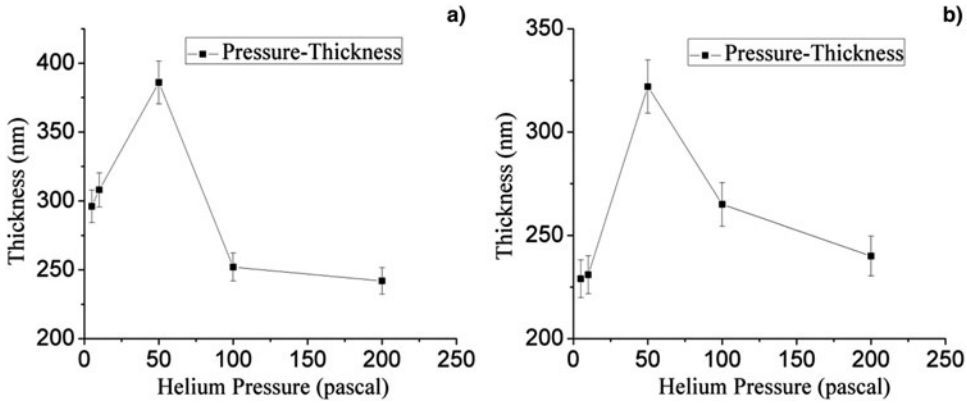

Fig. 9. Variation of thickness of PLD Mo thin film as a function of pressure (**a**) D_{TS} 0.03m, (**b**) D_{TS} 0.04m.

https://doi.org/10.1017/S0263034612000560 Published online by Cambridge University Press

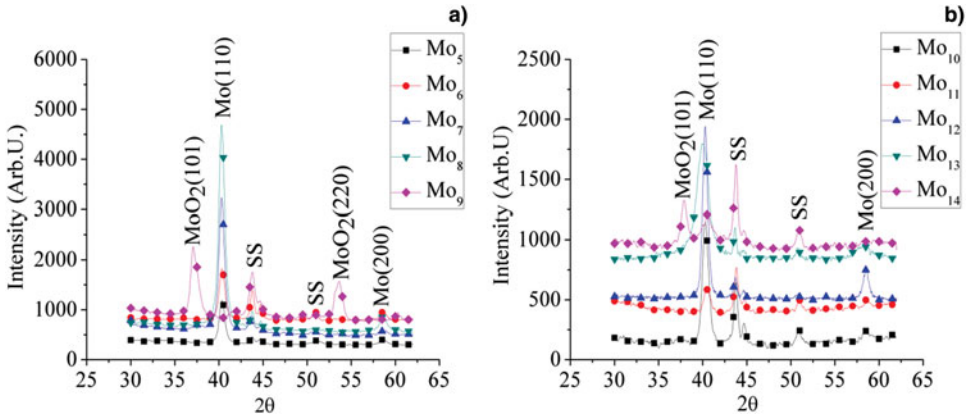

Fig. 10. (Color online) XRD patterns of samples (**a**) Mo_5 to Mo_9 and (**b**) Mo_{10} to Mo_{14}.

species of Mo at D_{TS}: 4 cm under 100 Pascal helium ambient, which is not sufficient to attain supper-saturation temperature for pure crystalline growth towards Mo (110) plane. XRD pattern of Mo_9 and Mo_{14} films clearly showed MoO_2 (101) and MoO_2 (220) crystal orientation. This is due to the oxygen impurity which becomes prominent at high pressure of 200 Pascal.

3.2.3. FIR and UV-visible Reflectivity

The specular FIR reflectivity of the Mo_5–Mo_9 and Mo_{10}–Mo_{14} are shown in Figure 11. The specular UV-visible reflectivities of the Mo_5–Mo_9, and Mo_{10}–Mo_{14}, respectively, are shown in Figure 12. The FIR reflectivity at $\lambda =$ 20 μm and UV-visible reflectivity at $\lambda = 840$ nm of Mo_5–Mo_9 and Mo_{10}–Mo_{14} are listed in Table 2. The film deposited at 50 Pascal background pressure had maximum FIR reflectivity, at $\lambda = 20$ μm about 98%, for both 0.03 m and 0.04 m target-substrate distance. It was observed that the film deposited at 5 Pascal background pressure had poor reflectivity for Mo_5 and Mo_{10} thin films. The maximum recorded specular reflectivity at $\lambda = 840$ nm, was about 84% for Mo_7–Mo_8 and about 87% for Mo_{12} thin films, respectively.

4. CONCLUSION

The detailed characterization of mirror like Mo thin films fabricated by PLD technique has been presented. The PLD Mo thin films were free from impurities: oxygen, carbon, and substrate elements. The formation of liquid droplets and hence large micro-structure were observed in the Mo thin films deposited at $D_{TS} \leq 0.02$ m. The surface morphology of the Mo mirrors improved with the increase of the target-substrate distance. The Mo films were predominately orientated in (110) plane at large target-substrate distance ($\geq$ 0.03 m). The Mo_4 mirror showing reflectivity 95 % at $\lambda = 20$ μm and 70% at $\lambda = 840$ nm is close to that of the polished bulk Mo mirror. The fringe visibility was observed to be improved with the increase of target-substrate distance. The crystallinity and the reflectivity were of the thin films was found to improved in presence of helium ambient. The thickness of the Mo thin films were observed to increase initially with the increase of background Helium

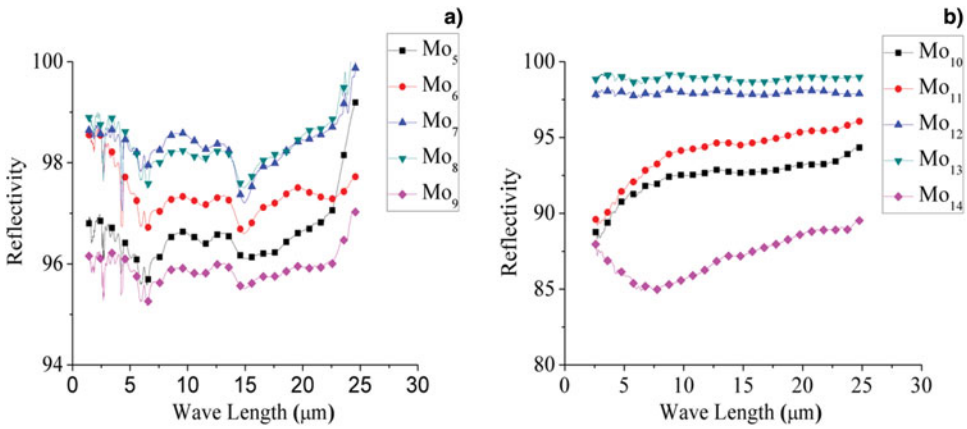

Fig. 11. (Color online) The specular FTIR reflectivity of the samples (**a**) Mo_5 to Mo_9 and (**b**) Mo_{10} to Mo_{14}.

https://doi.org/10.1017/S0263034612000560 Published online by Cambridge University Press

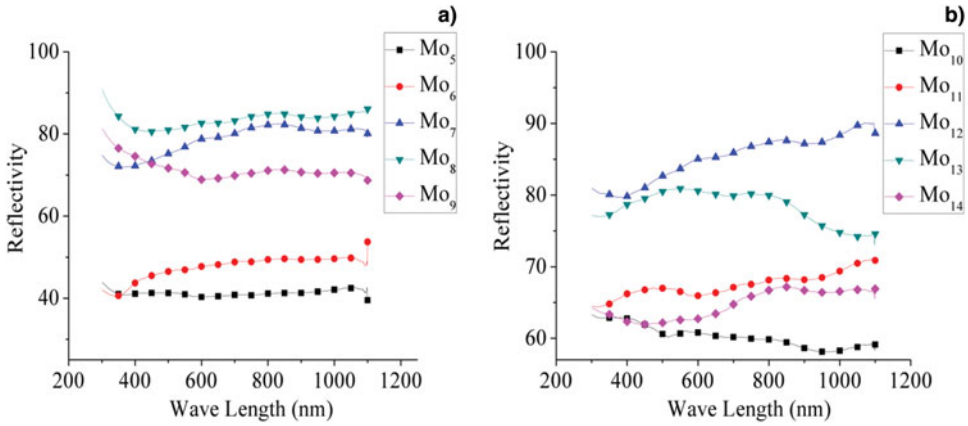

Fig. 12. (Color online) UV-visible reflectivity of the samples (**a**) Mo_5 to Mo_9 and (**b**) Mo_{10} to Mo_{14}.

pressure up to 50 Pascal and then falls down with further increase of background pressure to 200 Pascal. Mo_7 and Mo_{12} were the best thin films having reflectivity about 98% at $\lambda =$ 20 μm. At $\lambda = 840$ nm Mo_7 and Mo_{12} showed about 83% and about 87% reflectivity, respectively. These films also posses minimum FWHM for Mo (110) plane. Thus it can be concluded that the optimized parameters for obtaining mirror like quality PLD thin films of Mo having sufficient thickness about 300 nm for FM application are; 0.03–0.04 m target substrate distance, 50 Pascal Helium ambient, 500° C substrate temperature.

ACKNOWLEDGEMENT

This work is partially supported by BRFST, NFP (India), Project No. NFP/DIAG/01.

REFERENCES

Brailovsky, A.B., Gapnov, S.V. & Luchin, V.I. (1995). Mechanisms of melt droplets and solid-particle ejection from a target surface by pulsed laser action. *Appl. Phys. A* **61**, 81–86.

Culity, B.D. (1956). *Elements of X-Ray Diffraction*. Massachusetts: Addison-Wesley.

Djerdj, I., Tonejc, A.M., Tonejc, A. & Radic, N. (2005). XRD line profile analysis of tungsten thin films. *Vac*. **80**, 151–158.

Fruchart, O., Jaren, S. & Rothman, J. (1998). Growth modes of W and Mo thin epitaxial (110) films on (1120) sapphire. *Appl. Sur. Sci*. **135**, 218–232.

Gesheva, K.A. & Abrosimova, V. (1992). Rapid thermal annealing of CVD Mo thin films. *Bulgarian J. Phys*. **19**, 78–81.

Hernandez, M., Juarez, A. & Hernandez, R. (1999). Interferometric thickness determination of thin metallic films. *Superficies Y. Vacio*. **9**, 283–285.

Hirata, T. & Saito, K. (I990). The reflectance of sputtered molybdenum thin films implanted with nitrogen ions. *J. Mat. Sci. Lett.* **9**, 827–828.

Kamlesh, A. & Khare, A. (2005). Low-energy Low-divergence pulsed indium atomic beam by laser ablation. *Laser Part. Beams* **24**, 47–53.

Kamlesh, A. & Khare, A. (2006). Sculpted pulsed indium atomic beams via selective laser ablation of thin film. *Laser Part. Beams* **24**, 469–473.

Khatri, H. & Marsillac, S. (2008). The effect of deposition parameters on radiofrequency sputtered molybdenum thin films. *J. Phys. Condens. Mat*. **20**, 1–5.

Juppo, M., Vehkamaki, M., Ritala, M. & Leskela, M. (1998). Deposition of molybdenum thin films by an alternate supply of $MoCl_5$ and Zn. *J. Vac. Sci. Technol.* A **16**, 2845–2850.

Lam, Y.M., Tran, D.V. & Zheng, H.Y. (2007). A study of substrate temperature distribution during ultrashort laser ablation of bulk copper. *Laser Part. Beams* **25**, 155–159.

Lipa, M., Schunke, B., Gil, C., Bucalossi, J., Voitsenya, V. S., Konovalov, V., Vukolov, K., Balden, M., Temmerman, G.D., Oelhafen, P., Litnovsky, A. & Wienhold, P. (2006). Analyses of metallic first mirror samples after long term plasma exposure in Tore Supra. *Fusion Eng. Desi*. **81**, 221.

Marot, L., Temmerman, G.D., Thommen, V., Mathys, D. & Oelhafen, P. (2008). Characterization of magnetron sputtered rhodium films for reflective coatings. *Surf. Coat. Tech*. **202**, 2837–2843.

Nath, A. & Khare, A. (2011). Size induced structural modifications in copper oxide nanoparticles synthesized via laser ablation in liquids. *J. App. Phys*. **110**, 043111–043117.

Orlov, N.Y., Denisov, O.B., Rosmej, O.N., Schafer, D., Nisius, T., Wilhein, T., Zhidkov, N., Kunin, A., Suslov, N., Pinegin, A., Vatulin, V. & Zhao, Y. (2011). Theoretical and experimental studies of material radiative properties and their application to laser and heavy ion inertial fusion. *Laser Part. Beams* **29**, 69–80.

Roth, M., Brambrink, E., Audebert, P., Blazevic, A., Clarake, R., Cobble, J., Cowan, T.E., Fernandez, J., Fuchs, J., Geissel, M., Habs, D., Hegelich, M., Karsch, S., Ledingham, K., Neely, D., Ruhl, H., Schlegel, T. & Schreiber, J. (2005). Laser accelerated ions and electron transport in ultra-intense laser matter interaction. *Laser Part. Beams* **23**, 95–100.

Shena, Y.G., Mai, Y.W., Zhang, Q.C., Mckenzie, D.R., Mcfall, W.D. & Mcbride, W.E. (2000). Residual stress, microstructure, and structure of tungsten thin films deposited by magnetron sputtering. *J. Appl. Phys*. **87**, 177–187.

Tomachuk, C.R., De Rosa, L., Springer, J., Mitton, D.B., Saiello, S. & Bellucc, F. (2004). The wet corrosion of molybdenum thin film-Part II Behavior at 85°C. *Mat. Corrosion*. **55**, 665–670.

Voitsenya, V.S., Bardamid, A.F., Bondarenko, V.N., Jacob, W., Konovvalov, V.G., Masuzaki, S., Motojima, O., Orilinsikij,

https://doi.org/10.1017/S0263034612000560 Published online by Cambridge University Press

D.V., Poperenko, V.L., Ryzhokov, I.V., Sagara, A., Shtan, A.F., Solodovchenko, S.I. & Vinnichenko, M.V. (2001*a*). Some problems arising due to plasma-surface interaction for operation of the in-vessel mirrors in a fusion reactor. *J. Nucl. Mat.* **290**, 336–340.

Voitsenya, V., Costley, A.E., Bandourko, V., Bardamid, A., Bandourko, V., Hirooka, Y., Kasai, S., Klassen, N., Konovalov, V., Nagatsu, M., Orlinskij, D., Orsitto, F., Poperenko, L., Solodovchenko, S., Stan, A., Sugie, T., Taniguchi, M., Vinnichenko, M., Vukolov, K. & Zvonkov, S. (2001*b*). Diagnostic first mirrors for buring plasma experiments (invited). *Rev. Sci. Instrum.* **72**, 475–482.

Voitsenya, V.S., Konovalov, V.G., Shtan, A.F., Solodovchenko, S.I., Becker, M.F., Bardamid, A.F., Yakimov, K.I., Gritsyna, V.T. & Orlinskij, D.V. (1999). Some problems of the material choice for the first mirrors of plasma diagnostics in a fusion reactor. *Rev. Sci. Instrum.* **70**, 790–793.

Zhou, Y., Gao, B.Y., Jiao, Y.M., Deng, Z.C., Tang, Y.W., Yi, J., Tian, C.L., Ding, X.T. & Liu, Y. (2006). Study of first mirror exposure and protection in HL-2A tokomak. *Fusion Eng. Desi.* **81**, 2823–2826.

Wang, Y.L., Chen, C., Ding, X.C., Chu, L.Z., Deng, Z.C., Liang, W.H., Chen, J.Z. & Fu, G.S. (2011). Nucleation and growth of nanopartciles during pulsed laser deposition in an ambient gas. *Laser Part. Beams*. **29**, 105–111.

Wolowski, J., Badziak, J., Czarnecka, A., Parys, P., Pisarek, M., Rosinski, Turan, R., & Yerci, S. (2007). Application of pulsed laser deposition and laser-induced ion implantation for formation of semiconductor nano-crystallites. *Laser Part. Beams* **25**, 65–69.

https://doi.org/10.1017/S0263034612000560 Published online by Cambridge University Press